Numerical study on MHD flow and heat transfer of Maxwell hybrid nanofluid: A Caputo time fractional derivative model

Babitha^{a,*} and Madhura K R^b

^a Department of Mathematics, CHRIST University, Bangalore-560029, Karnataka, India

b Department of Sciences and Humanities, Swami Vivekananda Yoga Anusandhana Samsthana (S- VYASA)

Deemed to be University, Bangalore-560105, Karnataka, India

Abstract

The present mathematical framework theoretically investigates the impact of the fractional model on heat transfer advancement in mixed convection magnetohydrodynamics Maxwell hybrid nanofluid flow througha bi-directional stretching sheet. A Caputo-time derivative model is adopted in the work to inspect the behavior of fractional parameters on flow and heat transfer properties. Nanoparticles like copper and titanium dioxide, and base fluid water are considered for forming a hybrid nanofluid. Also, magnetic, buoyancy, and heating effects are considered. A system of non-linear coupled governing equations with the model of Caputo-time fractional derivative is subjected to non-dimensional forms by inserting appropriate non-dimensional quantities. Numerical results for the developing non-linear problem are acquired using a finite difference approximation technique together with the L1 algorithm. The impact of the involved flow influential elements on heat transfer and flow characteristics is analyzed and portrayed graphically. From the study, it is identified that the strengthening of fluid flow of hybrid nanofluid is directly correlated with the order of fractional derivatives, and the reverse trend is observed in thermal distribution.

Keywords: Maxwell bybrid nanofluid, Finite difference method, Fractional model, Relaxation times,

Magnetohydrodynamics.

Corresponding Author

Email addresses: babitha. shashinath@christuniversity. in (Babitha), madhura kr@svyasa. edu. in (Madhura KR)

Preprint submitted to Scientia Iranica

1. Introduction

Modern advances in nanotechnology have led to the discovery that the thermophysical characteristics of fluids fundamentally alter with the suspension of traditional nanoparticles/base fluids, which form nanofluids. In1995, Choi came up with the term "nanofluid" [1]. Vemula et al. [2] have discussed a numerical model of transient natural convection flow of nanofluid with variable surface thermal distribution. A review on the flow ofmagnetohydrodynamics (MHD) nanofluids with radiation effect over a vertical plate is carried out by Sheela et al. [3]. The thermal and mass transfers effect of a 3rd-grade nanofluid past a convectively heated surface undermagnetic impact is examined by Ali et al. [4]. Khan et al. [5] have analyzed entropy generation and thermal radiation effects on the flow of Sutterby nanofluid. Xiong et al. [31] studied the heat transfer and flow characteristics of couple-stress nanofluid with thermal conductivity and thermal radiations, variable viscosity, and non-uniform magnetic field effects. A critical insight into nanofluids for heat transfer enhancement is carried out by Alami et al. [6]. The thermally generated bioconvection flow of Williamson nanoliquid across an inclined stretched cylinder with linear mixed convection and a non-uniform heat sink/source was examined by Zhou et al. [32] using the bioconvection phenomena, suspension of gyrotactic microorganisms, and the activation energy is explained. In addition to continuing to employ these fluids, researchers have also been using a new category of nanofluids termed "hybrid" nanofluids (HNFs), which are obtained by suspension of nanoparticles or composites of distinct metals into the traditional(base) fluids. These HNFsare better and more stable than ordinary nanofluids. It is undeniable that the supplement of nanoparticles improved the thermal conductivity of base fluids, but it also caused issues along with stability, erosion, pressure drop, convection heat transfer, and pumping power, because the viscosity was improved as a resultof the formation of clusters, which increased the hydrodynamic diameter and decreased the specific surfacearea. In comparison to conventional fluids and the majority of unitary nanofluids, the hybrid nanofluids showed increased viscosity. Hybrid nanofluids offer improved rheological characteristics and cause less pipe blockage. Abiddin and Bachok have examined the impacts of $Al_2O_3 - TiO_2/H_2O$ hybrid nanofluidon heat transfer of steady-state laminar flow, and also discussed the stability of the dual solutions. The mixed convection flow and heat transfer of Ag-TiO₂/H₂O hybrid nanofluid is analyzed by Bakar et al. [7] with the impact of magnetic and radiation. A numerical illustration of boundary layer and MHD flow of Ag-TiO2/H₂O hybrid nanofluid in an irregular channel was reported by Kalpana et al. [8], and they discussed the impact of thermophoresis effect and Brownian motion in the heat transfer process. Few experimental and theoretical works on hybrid nanofluid under various circumstances were reported by several researchers [[9], [10], [11], [12], [13], [33]]. Also, to evaluate the impact of fluid viscosity and elastic behavior on flow nature, Maxwell suggested one of the most straightforward viscoelastic fluid models. This type of fluid is widely known as Maxwell fluid, and the associated model is the Maxwell fluid model. Several authors adopted the Maxwell model to inspect the flow behavior of hybrid nanofluids under various circumstances[[14], [15], [16]].

However, in the aforementioned works, the fractional derivatives involved in the governing equations have not be

considered in the classical study of nanofluids/hybrid nanofluids. The majority of research works are restricted to models of integer order. However, the fractional model becomes more significant as a resultof its role in explaining the intricate behavior of materials, notably long-term memory on fluid properties. Few works in this area have recently received notification. Using Caputo-time fractional derivatives, Aman et al. [17] investigated the impact of heat and mass transfer on a graphene-sodium alginate nanofluid. They also discussed about improvement of heat transfer by using mixed convection MHD Poiseuille flow of graphene- water nanofluid in a vertical channel [18]. Madhura et al. [19] have demonstrated analytical computation to study the heat transfer and flow characteristics of three distinct water-based fractional nanofluids and showed that containing Copper-water nanofluid displays a higher heat transfer rate in the existence and absence of thermal radiation. Few research works on fractional nanofluids have been carried out by the researchers in various aspects [[20], [21], [22], [34], [35], [36]].

The prime goal of the study is to accomplish numerical computation to find the results of unsteady, two-dimensional, laminar flow and heat transfer of Maxwell hybrid nanofluid across a vertical plate. The advanced model is accomplished with the supplement Caputo derivative and fractional relaxation times in the conventional model. Additionally, consideration is given to the effects of Ohmic heating, magnetic field, and internal heat production/absorption. The study adopts relaxation times (λ_1 , λ_2) and fractional parameters (α , β) of velocity and temperature, respectively, to control the mechanism of the considered mathematical model. Flow and heat transfer characteristics are simulated using the L1 algorithm (for fractional derivatives) and finite difference approximation (FDA) (for derivatives of integral orders). The impact of the governing parameters is elucidated with the aid of plots and tables.

The overview of the presentation of the article is as follows: Section 2 includes the flow and mathematical description. The numerical procedure and convergence criteria of the FDM are illustrated in Section 3.Section 4 comprises detailed explanations of the impact of flow parameters on the flow phenomena. Section5 gives the overall conclusions drawn from the investigation.

The outcomes of the present study have significant consequences for various advanced technologies due to the consideration of memory effect, different nanoparticles, and non-Newtonian behaviour. This work provided a framework for fluid flow and heat transport in critical engineering systems, and a few of them are listed below:

- High-performance heat exchangers: The strengthening of thermal profiles with increasing Eckert number (Ec) and internal heat generation (Q) upholds the design of compact heat exchangers capable of handling high thermal loads in metal casting, chemical processing, and power electronics cooling.
- Fractional time effects in transient cooling: The Caputo derivative allows for more accurate modeling of transient heat transfer, making it valuable for processes where rapid thermal response is critical, such as laser machining, quenching, or cryogenic applications.

2. Mathematical Formulation

Maxwell viscoelastic fluid's constitutive relationship to fractional order derivatives is [23]:

$$\tau + \lambda^a \frac{d^a t}{dt^a} = \mu \frac{d^\beta \xi}{dt^\beta},\tag{1}$$

where μ, ξ, λ , and τ denotes viscosity, shear strain, relaxation time, and shear stress, respectively, the time-

fractional Caputo derivatives with respect to $\frac{d^{\alpha}}{dt^{\alpha}}$ and $\frac{d^{\beta}}{dt^{\beta}}$, governed by fractional orders α and β , respectively.

According to the definition of the Caputo-time derivative with fractional order α is given as [24]:

$$\frac{d^{\alpha}}{dt^{\alpha}}h(t) = \frac{1}{\Gamma(1-\alpha)} \int_{0}^{t} \frac{\partial h(y,p)}{\partial p} (t-p)^{-\alpha} dp, \ \alpha \in [0,1].$$
 (2)

For $\beta = 1$, Eq. (1) reduces to a form that characterizes fluid-like behavior, as presented in Friedrich (1991), and can be written as:

$$\tau + \lambda^{\alpha} \frac{d^{\alpha} \tau}{dt^{\alpha}} = \mu \frac{d\xi}{dt}, \quad 0 \le \alpha \le 1.$$
 (3)

Setting $\alpha = 0$ in Eq. (3) yields the classical Newtonian fluid model, and conversely, when $\alpha = 1$ Eq. (3) corresponds to the ordinary Maxwell fluid model. These are given respectively by:

$$\tau = \mu \frac{d\xi}{dt},\tag{4}$$

$$\tau + \lambda \frac{d\tau}{dt} = \mu \frac{d\xi}{dt}.$$
 (5)

Unsteady, two-dimensional MHD boundary layer flow of Maxwell hybrid nanofluid through a stretching sheet is considered. The velocity region is taken as bi-directional across a stretching sheet, and mathematically, it is portrayed as U = [u(x, y, t), v(x, y, t), 0]. The velocity in the x-direction, whereas the y-axis extends upward and perpendicular to the plate as shown in Figure 1. The uniform magnetic field B_0 is employed normal to the fluid flow direction. At the beginning (t = 0), the sheet is invariant with the persistent environmental temperature θ_{∞} . Subsequently, once t > 0 then the plate setup into the movement with constant velocity U_0 and thermal distribution lowered or raised to θ_w . In this study, copper (Cu) and titanium dioxide (TiO₂) nanoparticles are introduced into a conventional base fluid, water (H₂O). It is assumed that the nanoparticles and the base fluid are in thermal equilibrium. The thermophysical characteristics of both the base fluid and the nanoparticles at a specified reference temperature are presented in Table 1.

The effective co-relations of hybrid nanofluids are given in Table 2. Utilizing Eq. (3) and the governing equations present model are given by [25]:

$$\frac{\partial U}{\partial x} + \frac{\partial V}{\partial y} = 0,\tag{6}$$

$$\left(1+\lambda_{1}^{\alpha}\frac{\partial^{\alpha}}{\partial t^{\alpha}}\right)\left(\frac{\partial U}{\partial t}+U\frac{\partial U}{\partial x}+V\frac{\partial U}{\partial y}\right)=v_{hnf}\frac{\partial^{2} U}{\partial y^{2}}+\frac{\sigma_{f}}{\rho_{f}}\left(1+\lambda_{1}^{\alpha}\frac{\partial^{\alpha}}{\partial t^{\alpha}}\right)UB_{0}^{2}+g\beta_{Thnf}\left(1+\lambda_{1}^{\alpha}\frac{\partial^{\alpha}}{\partial t^{\alpha}}\right)(\theta-\theta_{\infty}) (7)$$

$$\left(1 + \lambda_{2}^{\beta} \frac{\partial^{\beta}}{\partial t^{\beta}}\right) \left(\frac{\partial \theta}{\partial t} + U \frac{\partial \theta}{\partial x} + V \frac{\partial \theta}{\partial y}\right) = k_{hnf} \frac{\partial^{2} \theta}{\partial y^{2}} + \frac{\sigma_{f}}{(C_{p}\rho)_{f}} \left(1 + \lambda_{2}^{\beta} \frac{\partial^{\beta}}{\partial t^{\beta}}\right) U^{2} B_{0}^{2} + \frac{Q_{0}}{(C_{p}\rho)_{f}} \times \left(1 + \lambda_{2}^{\beta} \frac{\partial^{\beta}}{\partial t^{\beta}}\right) (\theta - \theta_{\infty})$$
(8)

Eqs. (6)-(8) are solved and subjected to the following conditions [19]:

$$V(x, y, t) = 0, \quad U(x, y, t) = 0, \quad \theta(x, y, t) = \theta_{\infty} \quad at \quad t \le 0,$$

$$V(x, 0, t) = 0, \quad U(x, 0, t) = \frac{xU_0}{L}, \quad \theta(x, 0, t) = \theta_{w} \quad \text{for } t > 0,$$

$$V(0, y, t) = 0, \quad U(0, y, t) = 0, \quad \theta(0, y, t) = \theta_{\infty} \quad \text{for } t > 0,$$

$$V(x, y, t) = 0, \quad U(x, y, t) = 0, \quad \theta(x, y, t) = \theta_{\infty} \quad as \quad y \to \infty.$$

Nondimensionalize Eqs. (6)-(8) utilizing the scaling as follows:

$$x^* = \frac{v_f}{U_0 L^2} x, \quad U^* = \frac{U}{U_0}, \quad y^* = \frac{y}{L}, \quad V^* = \frac{LV}{v_f}, \quad t^* = \frac{v_f t}{L^2}, \quad \theta^* = \frac{\theta - \theta_{\infty}}{\theta_{\omega} - \theta_{\infty}}, \quad \lambda_1^* = \frac{v_f}{L^2} \lambda_1, \quad \lambda_2^* = \frac{v_f}{L^2} \lambda_2.$$
 (9)

Use Eq. (9) in Eqs. (6)-(8) and neglecting *'s, one can get the non-dimensional structure of the governing equations as below:

$$\frac{\partial U}{\partial x} + \frac{\partial V}{\partial y} = 0,\tag{10}$$

$$\left(1 + \lambda_{1}^{\alpha} \frac{\partial^{\alpha}}{\partial t^{\alpha}}\right) \left(\frac{\partial U}{\partial t} + U \frac{\partial U}{\partial x} + V \frac{\partial U}{\partial y}\right) = X_{1} \frac{\partial^{2} U}{\partial y^{2}} + \frac{H}{X_{1}} \left(1 + \lambda_{1}^{\alpha} \frac{\partial^{\alpha}}{\partial t^{\alpha}}\right) U + \frac{Gr}{Re} \left(1 + \lambda_{1}^{\alpha} \frac{\partial^{\alpha}}{\partial t^{\alpha}}\right) \theta \tag{11}$$

$$\left(1 + \lambda_{2}^{\beta} \frac{\partial^{\beta}}{\partial t^{\beta}}\right) \left(\frac{\partial \theta}{\partial t} + U \frac{\partial \theta}{\partial x} + V \frac{\partial \theta}{\partial y}\right) = \frac{1}{Pr} \frac{\kappa_{hnf}}{\kappa_{f}} \frac{\partial^{2} \theta}{\partial y^{2}} + HEc \left(1 + \lambda_{2}^{\beta} \frac{\partial^{\beta}}{\partial t^{\beta}}\right) U^{2} + Q \left(1 + \lambda_{2}^{\beta} \frac{\partial^{\beta}}{\partial t^{\beta}}\right) \theta, \quad (12)$$

and the problem is subject to the following boundary conditions:

$$V(x, y, t) = 0, \quad U(x, y, t) = 0, \quad \theta(x, y, t) = 0 \quad at \quad t \le 0,$$

$$V(x, 0, t) = 0, \quad U(x, 0, t) = x \operatorname{Re}, \quad \theta(x, 0, t) = 1 \quad \text{for } t > 0,$$

$$V(0, y, t) = 0, \quad U(0, y, t) = 0, \quad \theta(0, y, t) = 0 \quad \text{for } t > 0,$$

$$V(x, y, t) = 0, \quad U(x, y, t) = 0, \quad \theta(x, y, t) = 0 \quad as \quad y \to \infty.$$
(13)

where

$$X_{1} = \frac{\rho_{f}}{\rho_{hnf} (1 - \phi_{1} - \phi_{2})^{2.5}}, Gr = \frac{g \beta_{Thnf} L^{3} (\theta_{w} - \theta_{\infty})}{v_{f}^{2}}, Re = \frac{LU_{0}}{v_{f}}, H = \frac{\sigma_{f} B_{0}^{2} L^{2}}{\mu_{f}}, Pr = \frac{v_{f}}{k_{hnf}}, Q = \frac{Q_{0} L^{2}}{\mu_{f} (C_{p})_{f}}.$$

2.1 Determination of Skin Friction and Nusselt Number Near the Plate

Surface drag C_f and the heat transfer rate (Nusselt number) Nu, which compute the viscous shear stress and rate of heat transfer individually, are significant physical quantities in assessing the flow and heat transfer properties of the fluid. For an integer order model, the expressions for local skin friction, C_f and heat transfer rate, Nu are presented by:

$$C_f = \frac{\mu}{\rho U_0^2} \left[\frac{\partial U}{\partial y} \right]_{y=0}, \quad Nu = -\frac{x}{\theta_w - \theta_\infty} \left[\frac{\partial \theta}{\partial y} \right]_{y=0}. \tag{14}$$

For the fractional model, C_f and Nu given by Eq. 17 can be modified as follows:

$$\left(1 + \lambda_1^{\alpha} \frac{\partial^{\alpha}}{\partial t^{\alpha}}\right) C_f = \frac{2\mu_{hnf}}{\rho U_0^2} \left[\frac{\partial U}{\partial y}\right]_{y=0}, \qquad \left(1 + \lambda_2^{\beta} \frac{\partial^{\beta}}{\partial t^{\beta}}\right) Nu = -\frac{k_{hnf} x}{k_f \Delta \theta} \left[\frac{\partial \theta}{\partial y}\right]_{y=0}. \tag{15}$$

Mean local skin-friction and heat transfer rate are presented by:

$$\left(1 + \lambda_1^{\alpha} \frac{\partial^{\alpha}}{\partial t^{\alpha}}\right) C_f = \frac{2\mu_{hnf}}{\rho U_0^2} \int_0^1 \left[\frac{\partial U}{\partial y}\right]_{y=0} dx, \quad \left(1 + \lambda_2^{\beta} \frac{\partial^{\beta}}{\partial t^{\beta}}\right) Nu = -\frac{k_{hnf} x}{k_f \Delta \theta} \int_0^1 \left[\frac{\partial \theta}{\partial y}\right]_{y=0} dx. \tag{16}$$

It is important to note that C_f and Nu for a conventional Maxwell hybrid nanofluid can be recovered as a special case by setting $\alpha = 1$ and $\beta=1$.

3. Numerical Approach and Simulation Outcomes

To address the coupled, nonlinear, and time-dependent magnetohydrodynamic (MHD) boundary layer equations incorporating fractional derivatives, a numerical method is developed in this section. The solution strategy combines the finite difference approach (FDA) with the L1 algorithm to handle the temporal fractional derivatives effectively. By employing Eq. (13), the system of Eqs. (10)–(12) is discretized and solved using the FDA framework as described in [26], integrated with the L1 approximation scheme. This hybrid technique ensures accurate treatment of the fractional-order terms while maintaining computational efficiency.

To implement the FDA, the computational domain in the x, y, and t directions is uniformly discretized into N, M, and K subintervals, respectively. The corresponding step sizes are denoted as Δx , Δy and Δt . The discrete grid points are defined as:

$$x_i = \Delta x, i = 0,1,2,3,...N$$

 $y_j = j\Delta y, j = 0,1,2,3,...M$
 $t_k = k\Delta t, k = 0,1,2,3,...K$

At each grid node (x_i, y_j, t_k) , the dependent variables $\psi \in \{U, V, T\}$ are represented by $\psi_{i,j}^k$, indicating their numerical values at that point in space and time.

The time-fractional derivative is approximated using the L1 algorithm, which provides a first-order accurate discretization for the Caputo fractional derivative and is provided by [22]:

$$\frac{\partial^{\lambda} g(t_{k})}{\partial t^{\lambda}} = \frac{\lambda t^{-\lambda}}{\lambda (2 - \lambda)} \sum_{s=0}^{k-1} \lambda_{s} \left[g(t_{k-s}) - g(t_{k-s-1}) \right] + O(\Delta t^{2-\lambda}),$$

$$= \frac{\lambda t^{-\lambda}}{\lambda (2 - \lambda)} \left[g(t_{k}) - \lambda g(t_{0}) - \sum_{s=0}^{k-1} (\lambda_{s-1} - \lambda_{s}) g(t_{k-s}) \right] + O(\Delta^{2-\lambda}),$$
(17)

where
$$\lambda_s = (s+1)^{1-\lambda} - s^{1-\lambda}, s=0,1,2,3,...$$

The relationship below is derived based on the fundamental properties of the Caputo time-fractional derivative

$$\frac{\partial^{\lambda+1} g(t_k)}{\partial t^{\lambda+1}} = \frac{\partial^{\lambda} g'(t_k)}{\partial t^{\lambda}},\tag{18}$$

Where
$$g'(t_k) = \frac{g(t_k) - g(t_{k-1})}{\Delta t}$$
.

Finite difference approximations for partial order derivatives of those that appeared in Eqs. (10)-(12) at the node (x_i, y_i, t_k) :

$$\frac{\partial U}{\partial t}\Big|_{t=t_{k}} = \frac{U_{i,j}^{k} - U_{i,j}^{k-1}}{\Delta t} + O(\Delta t),$$

$$U \frac{\partial U}{\partial x}\Big|_{t=t_{k}} = U_{i,j}^{k-1} \frac{U_{i,j}^{k} - U_{i-1,j}^{k}}{\Delta x} + O(\Delta x),$$

$$V \frac{\partial U}{\partial y}\Big|_{t=t_{k}} = V_{i-1,j}^{k} \frac{U_{i,j}^{k} - U_{i,j-1}^{k}}{\Delta y} + O(\Delta y),$$

$$\frac{\partial^{2} U}{\partial y^{2}}\Big|_{t=t_{k}} = \frac{U_{i,j+1}^{k} - 2U_{i,j}^{k} + U_{i,j-1}^{k} + U_{i,j-1}^{k-1} - 2U_{i,j}^{k-1} + U_{i,j+1}^{k-1}}{2\Delta y^{2}} + O(\Delta y^{2}),$$

(19)

Numerical solution of the unsteady coupled nonlinear differential equations is obtained in the succeeding section. By substituting Eq. (21) along with Eq. (23) into the governing Eqs. (10)–(12), the system is transformed into a set of algebraic equations, expressed as follows:

$$\left[\frac{1+r_{2}}{\Delta t} + \frac{1+r_{2}}{\Delta x}U_{i,j}^{k-1} + \frac{1+r_{2}}{\Delta y}V_{i,j}^{k-1} + 2K_{2} - Q\frac{2+r_{2}}{2}\right]\theta_{i,j}^{k} = K_{2}\theta_{i,j+1}^{k} + \frac{1+r_{2}}{\Delta x}U_{i,j}^{k-1}\theta_{i-1,j}^{k} + \left[\frac{1+r_{2}}{\Delta y}V_{i,j}^{k-1} + K_{2}\right]\theta_{i,j-1}^{k} + \left[\frac{1+r_{2}}{\Delta t} - 2K_{2} + \frac{Qr_{2}}{2}\right]\theta_{i,j}^{k-1} + K_{2}\theta_{i,j-1}^{k-1} + K_{2}\theta_{i,j+1}^{k-1} + \left[\left(\frac{B_{1}}{\Delta t} + \frac{B_{2}}{\Delta x} + \frac{B_{3}}{\Delta y} - \frac{QB_{5}}{2}\right)r_{2}\right] + \text{HEc}\left(1+r_{2}\right)U_{i,j}^{k}U_{i,j}^{k} + \text{HEc}\,\,r_{2}\left(U_{i,j}^{k}\right)U_{i,j}^{k-1} - \text{HEc}\,\,r_{2}\left(r_{2}B_{4}\right)U_{i,j}^{k},$$

$$\left[\frac{1+r_{1}}{\Delta t} + \frac{1+r_{1}}{\Delta x}U_{i,j}^{k-1} + \frac{1+r_{1}}{\Delta y}V_{i,j}^{k-1} + 2K_{1} + X_{1} \frac{2+r_{1}}{2}\right]U_{i,j}^{k} = K_{1}U_{i,j+1}^{k} + \frac{1+r_{1}}{\Delta x}U_{i,j}^{k-1}U_{i-1,j}^{k} + K_{1}U_{i,j+1}^{k-1} + U_{i,j+1}^{k} + U_{i,j+1}^{k} + U_{i,j+1}^{k} + U_{i,j+1}^{k} + U_{i,j+1}^{k} + V_{1}U_{i,j+1}^{k} + V_{1}U$$

$$V_{i,j}^{k} = V_{i,j-1}^{k-1} + V_{i,j-1}^{k} - V_{i,j}^{k-1} + \frac{\Delta y}{2\Delta x} \left[U_{i-1,j-1}^{k} + U_{i-1,j}^{k} - U_{i,j-1}^{k} - U_{i,j}^{k} + U_{i-1,j-1}^{k-1} + U_{i-1,j}^{k-1} - U_{i,j-1}^{k-1} \right], \tag{22}$$

Where

$$K_{1} = \frac{X_{1}}{2\Delta y^{2}}, r_{1} = \frac{\lambda_{1}^{\alpha} \Delta t^{-\alpha}}{\lambda (2-\alpha)}, r_{2} = \frac{\lambda_{1}^{\beta} \Delta t^{-\beta}}{\lambda (2-\beta)}, K_{2} = \frac{v_{hnf}}{2k_{f} Pr \Delta y^{2}}$$

$$A_{1} = \sum_{s=1}^{k-1} (\alpha_{s-1} - \alpha_{s}) \left(U_{i,j}^{k-s} - U_{i,j}^{k-s-1} \right), A_{2} = \sum_{s=1}^{k-1} (\alpha_{s-1} - \alpha_{s}) U_{i,j}^{k-s-1} \left(U_{i,j}^{k-s} - U_{i-1,j}^{k-s} \right),$$

$$A_{3} = \sum_{s=1}^{k-1} (\alpha_{s-1} - \alpha_{s}) V_{i,j}^{k-s-1} \left(U_{i,j}^{k-s} - U_{i,j-1}^{k-s} \right), A_{4} = \sum_{s=1}^{k-1} (\alpha_{s-1} - \alpha_{s}) \left(U_{i,j}^{k-s} + U_{i,j}^{k-s-1} \right),$$

$$A_{5} = \sum_{s=1}^{k-1} (\alpha_{s-1} - \alpha_{s}) \left(\theta_{i,j}^{k-s} + \theta_{i,j}^{k-s-1} \right), B_{1} = \sum_{s=1}^{k-1} \left(\beta_{s-1} - \beta_{s} \right) \left(\theta_{i,j}^{k-s} - \theta_{i,j}^{k-s-1} \right),$$

$$B_{2} = \sum_{s=1}^{k-1} \left(\beta_{s-1} - \beta_{s} \right) U_{i,j}^{k-s-1} \left(\theta_{i,j}^{k-s} - \theta_{i-1,j}^{k-s} \right), B_{3} = \sum_{s=1}^{k-1} \left(\beta_{s-1} - \beta_{s} \right) V_{i,j}^{k-s-1} \left(\theta_{i,j}^{k-s} - \theta_{i,j-1}^{k-s} \right),$$

$$B_{4} = \sum_{s=1}^{k-1} \left(\beta_{s-1} - \beta_{s} \right) \left(U_{i,j}^{k-s} + U_{i,j}^{k-s-1} \right), B_{5} = \sum_{s=1}^{k-1} \left(\beta_{s-1} - \beta_{s} \right) \left(\theta_{i,j}^{k-s} + \theta_{i,j}^{k-s-1} \right).$$

Discretized forms of the skin friction coefficient and Nusselt number are given below

$$C_{f} = \frac{1}{1+r_{1}} \left[r_{1} \sum_{s=1}^{k-1} C_{f} \left(t_{k-s} \right) \left(\alpha_{s-1} - \alpha_{s} \right) + \frac{2}{Re(1-\phi)^{2.5}} \int_{0}^{1} \left[\frac{\partial U}{\partial y} \right]_{y=0} dx \right], \tag{24}$$

$$Nu = \frac{1}{1 + r_2} \left[r_2 \sum_{s=1}^{k-1} (\beta_{s-1} - \beta_s) Nu(t_{k-s}) - \frac{k_{hnf}}{k_f} \int_0^1 \left[\frac{\partial \theta}{\partial y} \right]_{y=0} dx \right].$$
 (25)

The computational region is defined as a rectangular region with $x_{max}=1$ and $y_{max}=10$. The value of y_{max} is chosen sufficiently large to approximate the condition $y\to\infty$, ensuring that the far-field boundary lies outside the boundary layer region. The region is uniformly discretized into M and N sub-intervals along the x and y directions, respectively. At a given time level, the numerical solution is represented as a three-dimensional matrix of size $M\times N\times K$, where K denotes the number of time steps. For various values of parameters and grid sizes, governing equations are solved. From the computation, it is noted that the temperature and velocity values remain unaltered for the mesh size $\Delta t=0.05$, $\Delta x=\Delta y=0.05$ and $\Delta t=0.01$, $\Delta x=\Delta y=0.01$. Furthermore, the profile values are convergent in the considered range of parameters. In the numerical simulations, the time step and spatial grid sizes are chosen based on convergence criteria, accuracy, and computational efficiency. Accordingly, the step sizes are set as $\Delta t=0.05$, $\Delta x=0.05$, and $\Delta y=0.05$. The variations in fluid motion and temperature across the xy-plane is analysed through three-dimensional graphical representations. These plots demonstrate good numerical stability and convergence in both time and space. The corresponding results are illustrated in figures 2 and 3.

4. Results and discussion

The primary objective of the work is to examine the effects of magnetrohydrodynamics flow and heat transfer properties of fractional Maxwell HNF over a bidirectional stretching sheet. A MATLAB code has been developed to simulate the governing Eqs. (24)-(26) utilizing FDA and an amalgamated L1 algorithm, and to obtain the outcomes of industrial needs. A theoretical study is carried out to demonstrate a few important physical aspects of the procured results. The variation of fluid flow, thermal, skin friction coefficient and the heat transfer rate is described in detail and displayed in plots 2 - 15 and tables 1 - 4 when different values of flow-controlling parameters, such as fractional parameters (α , β), magnetic parameter (H), Eckert number (Ec), momentum and thermal relaxation times (λ 1, λ 2), volume fraction of nanoparticle (ϕ) and heat source/sink parameter (Q) are employed. Table 5 provides a comparative study between the present model and Turkyilmazoglu and Pop [30] in the absence of magnetic field, heat generation, and radiation effects, and the single-phase ordinary nanofluid model, and the results show good agreement. It is significant to note that the acquired results are consistent with the findings of previous studies to support their accuracy. For that, let's assume that the fractional parameter α , β and relaxation parameters equal to 1. This will result in a solution that has the same flow properties as ordinary nanofluids, and coincides with the work of Madhura et al. [37].

Figure 4 explains the change in velocity for the various fractional parameter α values. It is pointed out that when α increases, the velocity of the fluid increases and aids in controlling the fluid flow. Physically, it is trifling that the viscosity of the hybrid nanofluid will grow as α rises. Regular Maxwell HNFs have a densevelocity boundary layer, but classical Newtonian nanofluids display the strongest flow resistance, demonstrating that viscoelasticity increases flow defiance with the strength of α .

The velocity distribution for the various momentum relaxation time λ_1 is shown in Fig. 5. With an increase in λ_1 , the fluid motion slows down. As λ_1 increases, the thickness of the velocity boundary layer decreases, which results in a decrease in the properties of Maxwell viscoelastic HNF flow. At the other end, a rise in λ_1 causes an increase in the time it takes to react to an applied stress, which increases the resistance to fluid movement. Additionally, there is a relationship between λ_1 and the fluid's viscosity, which leads to a decline in the fluid's velocity as λ_1 grows. Especially considering that $\lambda_1 = 0$ yields the Newtonian nanofluidflow.

Figure 6 behavior of how the velocity distribution is affected when the applied magnetic field varies. Akind of drag force that is Lorentz force exerts when a transverse magnetic field B_0 , is employed to the fluidflow. Therefore, the fluid is restricted by the Lorentz force, which also diminishes the fluid flow momentum. Thus, the fluid velocity reduces with increasing magnetic parameter H, and the same is delineated in Fig. 6. Also, Fig. 7 portrays the influence of Grashof number Gr on fluid flow. It is observed that the rise in Gr leads to the strengthening of the velocity profile. It means, in terms of physics, that the Grashof number prioritizes buoyant force above viscous hydrodynamic force. For the higher values of Gr, viscous effects in the momentum equations are lessened; consequently, the fluid has more momentum.

The flow field of the model for different nanoparticle volume fractions ϕ is elucidated in Figure 8. ϕ is the sum

of nanoparticle volume fractions of first and second nanoparticles, i.e., $\phi = \phi_1 + \phi_2$. In this study, we have adopted the Maxwell model and observed that ϕ shows a crucial impact on the viscosity and thermal conductivity of the HNFs. The greater ϕ prompted the formation of larger nano-clusters because of VanderWaals forces among the particles that might increase viscosity by restricting the movement of fluid layers. Also, internal shear stress increased due to nanoparticle volume fraction, increasing the hybrid nanofluid's viscosity. Consequently, the velocity of the hybrid nanofluid reduces, and a similar nature is observed by Afrand et al. [27] and Esfe et al. [28].

Figure 9 demonstrates the influence of the fractional parameter β on the temperature profile. As fluid flow is controlled by α , the parameter β provides control of the heat flow. The temperature profile has significantly decreased, as evidenced by an improvement in the β . The relaxation time λ_2 on temperature distribution shows a similar tendency, and the same is seen in Fig. 10. The time gap for heat transmission from the heat source to the fluid flow area is improved as λ_2 increases, and as a result, the temperature distribution in that area decreases. The Newtonian nanofluid flow is described when λ_2 =0.

Figure 11 illustrates the influence of Eckert number Ec on the temperature of Maxwell hybrid nanofluid. Temperature rises for larger values of Ec, where Ec is a measure of the degree of Ohmic heating; a larger Ec indicates a stronger Ohmic heating. As a result, the heat transmission rate decreases while the heat dissipation rate increases. Consequently, the temperature rises.

To understand how the heat absorption coefficient Q affects the temperature distributions, it is important to understand that Q < 0 and Q > 0 denote the internal heat sink and heat source, respectively. Therefore, the Q values are taken as -1, 0, 1, 2 in Fig. 12. From this graph, it can be seen that an increasing Q results in an increase in the thermal distribution. This is because increasing Q > 0 releases energy, leading to an increase in the thermal distribution, while increasing values of Q < 0 absorb energy, leading to a decline in temperature.

Figure 13 displays the relationship between the dimensionless temperature profile versus nanoparticle volume fraction ϕ . It is observed that raising the volume fraction parameter makes the temperature profile to become more intense. The thermal conductivity of the hybrid nanofluid is improved by a greater volume percentage of nanoparticles, which thickens the thermal boundary layer. The ϕ is an important one that significantly affects how well the fluids conduct heat. Thus, we can conclude that the temperature can be adjusted in many industrial processes by altering the nanoparticle volume fraction. Similar behavior of nanofluid is observed by Colla et al. [29] experimentally.

Figures 14-15 are plotted to analyze the influence of the dispersion of the nanoparticle in the ordinary fluid on the flow velocity and temperature distribution by varying the volume fraction. In the current study, by taking either $\phi 1 = 0$ or $\phi 2 = 0$, we get the ordinary (or mono-type) nanofluid model from the hybrid nanofluid model. From Figure 14, it is noticed that the flow velocity of the HNF $(H_2O - (Cu + TiO_2))$ and ordinary nanofluid $(H_2O - Cu)$ is more significant compared to the base fluid (water). The enhanced thermal conductivity

is the reason for the cause. In addition, hybrid nanofluids are more stable compared to ordinary nanofluids. The fluid thermal conductivity improves the thermal distribution. Thus, the thickness of the thermal boundary layer increased for nanofluid and hybrid nanofluid, and the same is depicted in Fig. 15.

Key engineering quantities of interest, namely the skin friction coefficient (C_f) and the Nusselt number (Nu), are computed at the boundary surfaces and evaluated under varying flow control parameters. The corresponding numerical results are summarized in Tables 3 and 4. Analysis of the skinfriction coefficient is necessary since it contributes significantly to calculating the overall drag. Accurate skin friction measurement is essential for practical issues like improving vehicle fuel efficiency, describing the flow of a fluid across different solid geometries, etc. On the other hand, the Nusselt number produces the qualitative and quantitative properties of heat transfer studies. The effect of the fractional parameter, relaxation time, Grashof number, magnetic parameter, and nanoparticle volume fraction on surface drag is discussed in Table 3. As α and λ_1 increase, C_f also increases, but a reverse trend is observed for Gr because fluid particlesgain more velocity due to the rise in the Gr, this causes more heat to be lost to the environment, which lowers the skin friction coefficient. While the magnetic parameter and nanoparticle volume fraction elevates, C_f increases monotonically. It is evident that adding particles to any base fluid causes the viscosity to increase, and hybrid nanofluids exhibit a similar characteristic. As a result, the hybrid nanofluid's viscosity and frictional factor are both increased by the high nanoparticles volume fraction in the fluid. The influence of fractional parameter, Eckert number, relaxation time, heat generation parameter, and nanoparticle volume fraction on heat transfer rate is analysed, and the corresponding results are demonstrated in Table 4. Clearly, Nu declines with an increase of Q and Ec but enhances with an improvement in the β , ϕ , and λ_2 .

5. Conclusions

Utilizing the modern theory of Caputo time-fractional derivative for unsteady 2-dimensional boundarylayer flow and heat transfer analysis of Maxwell hybrid nanofluid, significant findings were discovered in this study. Time derivatives are replaced by Caputo fractional derivatives. The key findings from the analysisare:

- O The flow of hybrid nanofluid is favored with increasing α and Gr, whereas λ_1 and H oppose the fluid motion.
- Temperature profiles are strengthened remarkably with increasing Eckert number and heat source parameter. On the contrary, with increasing relaxation time and fractional parameter, the temperature diminishes.
- O Shear stress increases for the higher values of α , $\lambda 1$, and ϕ .
- o Increasing the values of the H, Ec, and Q significantly reduces the heat transfer rate, whereas the ϕ exhibits an opposite effect, enhancing the heat transfer.
- o The results for the Newtonian hybrid nanofluid can be recovered as a special case by setting the parameters

$$\lambda_1 = \lambda_2 = 0.$$

- The study disclosed that the consideration of a fractional model improves 13.367% of the heat transfer rate.
- Ordinary integer models take into account the instantaneous response to external forces, while fractional derivatives take into account the memory-dependent behavior of actual fluids and materials. This is especially important for viscoelastic fluids that show time-delayed stress-strain correlations, such as Maxwell fluids. Also, the consideration of hybrid nanofluid improves the thermal conductivity of the base fluid and which enhances the thermal conductivity due to synergistic effects between different particle types.

Nomenclature

Latin	sym	bo	ls
-------	-----	----	----

 B_0 magnetic field

Eckert number

H magnetic parameter

Pr Prandtl number

 C_p specific heat

 C_f skin-friction

Reynolds number

Q heat source/sink parameter

Grashof number

Nu Nusselt number

 Q_0 heat absorption/generation coefficient

L characteristics length

t time

g gravity

k thermal conductivity

U, V fluid flow along x and y axes

Greek symbols

α momentum fractional parameter

 β_T thermal expansion coefficient

λ relaxation time

v kinematic viscosity

β thermal energy fractional parameter

 λ_1 , λ_2 relaxation times of velocity and temperature

 μ dynamic viscosity

7 shear stress

 σ electric conductivity

 κ_T thermal diffusivity

 θ dimensionless temperature

 ξ shear strain

 ϕ nanoparticle volume fraction

ρ density

Subscripts or superscripts

hnf hybrid nanofluid

f base fluid

Declaration:

Availability of data and materials: Not applicable

Conflict of interest: The authors declare that they have no conflict of interest.

References

- [1] S. U. Choi, J. A. Eastman, Enhancing thermal conductivity of fluids with nanoparticles, TechnicalReport, Argonne National Lab. (ANL), Argonne, IL (United States), 1995.
- [2] Rajesh, V., Sheremet, M.A., and Öztop, H.F., "Impact of hybrid nanofluids on MHD flow and heat transfer near a vertical plate with ramped wall temperature", *Case Studies in Thermal Engineering*, **28**, p. 101557 (2021). https://doi.org/10.1016/j.csite.2021.101557
- [3] Shantha Sheela, J., Gururaj, A.D.M., Ismail, M., *et al.*, "Review on magnetohydrodynamic flow of nanofluids past a vertical plate under the influence of thermal radiation", *IOP Conference Series: Earth and Environmental Science*, **850**(1), p. 012037 (2021). https://doi.org/10.1088/1755-1315/850/1/012037
- [4] Ali, K., Faridi, A.A., Ahmad, S., Jamshed, W., et al. "Quasi-linearization analysis for heat and mass transfer of magnetically driven 3rd-grade (Cu–TiO₂/engine oil) nanofluid via a convectively heated surface", *International Communications in Heat and Mass Transfer*, 135, p. 106060 (2022). https://doi.org/10.1016/j.icheatmasstransfer.2022.106060
- [5] Alami, A.H., Ramadan, M., Tawalbeh, M., et al. Ayoub, M., Alashkar, A., Abdelkareem, M.A., and Olabi, A.G., "A critical insight on nanofluids for heat transfer enhancement", *Scientific Reports*, **13**(1), p. 15303 (2023). https://doi.org/10.1038/s41598-023-42489-0
- [6] Azeem Khan, W., Anjum, N., Hobiny, A., et al. "Entropy generation analysis for chemically reactive flow of Sutterby nanofluid considering radiation aspects", *Scientia Iranica*, 31(12), pp. 935–944 (2024). https://doi.org/10.24200/sci.2023.60105.6594
- [7] Bakar, S.A., Arifin, N.M., Bachok, N., and Ali, F.M., "Effect of thermal radiation and MHD on hybrid Ag—TiO₂/H₂O nanofluid past a permeable porous medium with heat generation", *Case Studies in Thermal Engineering*, **28**, p. 101681 (2021). https://doi.org/10.1016/j.csite.2021.101681
- [8] Kalpana, G., Madhura, K.R., and Kudenatti, R.B., "Impact of temperature-dependent viscosity and thermal conductivity on MHD boundary layer flow of two-phase dusty fluid through permeable medium", *Engineering Science and Technology, an International Journal*, **22**(2), pp. 416–427 (2019). https://doi.org/10.1016/j.jestch.2018.10.009
- [9] Gireesha, B.J., Sowmya, G., Khan, M.I., et al. "Flow of hybrid nanofluid across a permeable longitudinal moving fin along with thermal radiation and natural convection", *Computer Methods and Programs in Biomedicine*, **185**, p. 105166 (2020). https://doi.org/10.1016/j.cmpb.2019.105166
- [10] Vidhya, R., Balakrishnan, T., Kumar, B.S., et al. Angulo-Cabanillas, L., Shaik, S., Saleh, B., and Alarifi, I.M., "An experimental study of ZrO₂–CeO₂ hybrid nanofluid and response surface methodology for the prediction of heat transfer performance: The new correlations", *Journal of Nanomaterials*, **2022**(1), p. 6596028 (2022). https://doi.org/10.1155/2022/6596028
- [11] Ali, H.M., Hybrid nanofluids for convection heat transfer, Academic Press, (2020).
- [12] Sahoo, R.R., "Experimental study on the viscosity of hybrid nanofluid and development of a new correlation", *Heat and Mass Transfer*, **56**, pp. 3023–3033 (2020). https://doi.org/10.1007/s00231-020-02915-9
- [13] Mollamahdi, M., Abbaszadeh, M., and Sheikhzadeh, G.A., "Analytical study of Al₂O₃–Cu/water micropolar hybrid nanofluid in a porous channel with expanding/contracting walls in the presence of

- magnetic field", Scientia Iranica, 25(1), pp. 208–220 (2018). https://doi.org/10.24200/sci.2017.4250
- [14] Gul, T., Mukhtar, S., Alghamdi, W., et al. "The radiative flow of the thin-film Maxwell hybrid nanofluids on an inclined plane in a porous space", *Frontiers in Energy Research*, **10**, p. 970293 (2022). https://doi.org/10.3389/fenrg.2022.970293
- [15] Algehyne, E.A., El-Zahar, E.R., Elhag, et al. "Investigation of thermal performance of Maxwell hybrid nanofluid boundary value problem in vertical porous surface via finite element approach", *Scientific Reports*, **12**(1), p. 2335 (2022). https://doi.org/10.1038/s41598-022-06213-8
- [16] Chu, Y.M., Ali, R., Asjad, M.I., et al. "Heat transfer flow of Maxwell hybrid nanofluids due to pressure gradient into rectangular region", *Scientific Reports*, **10**(1), p. 16643 (2020). https://doi.org/10.1038/s41598-020-73174-1
- [17] Aman, S., Khan, I., Ismail, Z., et al. "Applications of fractional derivatives to nanofluids: exact and numerical solutions", *Mathematical Modelling of Natural Phenomena*, **13**(1), p. 2 (2018). https://doi.org/10.1051/mmnp/2018013
- [18] Aman, S., Khan, I., Ismail, Z., et al. "A new Caputo time fractional model for heat transfer enhancement of water-based graphene nanofluid: An application to solar energy", *Results in Physics*, **9**, pp. 1352–1362 (2018). https://doi.org/10.1016/j.rinp.2018.04.007
- [19] Madhura, K.R., Babitha, and Iyengar, S.S., "Analysis of heat transfer and thermal radiation on natural convective flow of fractional nanofluids", *Journal of Nanofluids*, **8**(5), pp. 1158–1169 (2019). https://doi.org/10.1166/jon.2019.1645
- [20] Shen, M., Chen, H., Zhang, M., et al. "A comprehensive review of nanofluids with fractional derivatives: Modeling and application", *Nanotechnology Reviews*, **11**(1), pp. 3235–3249 (2022). https://doi.org/10.1515/ntrev-2022-0496
- [21] Hasin, F., Ahmad, Z., Ali, F., et al. "A time fractional model of Brinkman-type nanofluid with ramped wall temperature and concentration", *Advances in Mechanical Engineering*, **14**(5), p. 16878132221096012 (2022). https://doi.org/10.1177/168781322210960
- [22] Babitha, Madhura, K.R., and Makinde, O.D., "Computational study on heat transfer and MHD-electrified flow of fractional Maxwell nanofluids suspended with SWCNT and MWCNT", *Heat Transfer*, **50**(6), pp. 5813–5834 (2021). https://doi.org/10.1002/htj.22150
- [23] Friedrich, C.H.R., "Relaxation and retardation functions of the Maxwell model with fractional derivatives", *Rheologica Acta*, **30**, pp. 151–158 (1991). https://doi.org/10.1007/BF01134604
- [24] Fetecau, C., Ellahi, R., and Sait, S.M., "Mathematical analysis of Maxwell fluid flow through a porous plate channel induced by a constantly accelerating or oscillating wall", *Mathematics*, **9**(1), p. 90 (2021). https://doi.org/10.3390/math9010090
- [25] Anwar, M.S., Ahmad, R.T.M., Shahzad, T., et al. "Electrified fractional nanofluid flow with suspended carbon nanotubes", *Computers & Mathematics with Applications*, **80**(5), pp. 1375–1386 (2020). https://doi.org/10.1016/j.camwa.2020.07.005

- [26] LeVeque, R.J., Finite difference methods for ordinary and partial differential equations: steady-state and time-dependent problems, SIAM, (2007). https://doi.org/10.1137/1.9780898717839.ch1
- [27] Afrand, M., Najafabadi, K.N., and Akbari, M., "Effects of temperature and solid volume fraction on viscosity of SiO₂-MWCNTs/SAE40 hybrid nanofluid as a coolant and lubricant in heat engines", *Applied Thermal Engineering*, **102**, pp. 45–54 (2016). https://doi.org/10.1016/j.applthermaleng.2016.04.002
- [28] Esfe, M.H., Rostamian, H., and Sarlak, M.R., "A novel study on rheological behavior of ZnO-MWCNT/10W40 nanofluid for automotive engines", *Journal of Molecular Liquids*, **254**, pp. 406–413 (2018). https://doi.org/10.1016/J.MOLLIQ.2017.11.135
- [29] Colla, L., Fedele, L., Scattolini, M., et al. "Water-based Fe₂O₃ nanofluid characterization: thermal conductivity and viscosity measurements and correlation", *Advances in Mechanical Engineering*, **4**, p. 674947 (2012). https://doi.org/10.1155/2012/674947
- [30] Turkyilmazoglu, M., and Pop, I., "Heat and mass transfer of unsteady natural convection flow of some nanofluids past a vertical infinite flat plate with radiation effect", *International Journal of Heat and Mass Transfer*, **59**, pp. 167–171 (2013). https://doi.org/10.1016/j.ijheatmasstransfer.2012.12.009
- [31] Xiong, P.Y., Nazeer, M., Hussain, F., et al. "Two-phase flow of couple stress fluid thermally effected slip boundary conditions: Numerical analysis with variable liquids properties", *Alexandria Engineering Journal*, **61**(5), pp. 3821–3830 (2022). https://doi.org/10.1016/j.aej.2021.09.012
- [32] Zhou, S.S., Khan, M.I., Qayyum, S., et al. "Nonlinear mixed convective Williamson nanofluid flow with the suspension of gyrotactic microorganisms", *International Journal of Modern Physics B*, **35**(12), p. 2150145 (2021). https://doi.org/10.1142/S0217979221501459
- [33] Sulochana, G., Prasad, C.V., Bhatti, S.K., et al. "Impact of multi-walled carbon nanotubes (MWCNTs) on hybrid biodiesel blends for cleaner combustion in CI engines", *Energy*, **303**, p. 131911 (2024). https://doi.org/10.1016/j.energy.2024.131911
- [34] Swetha, D.S., Madhura, K.R., Babitha, et al. "MHD Maxwell nanofluid flow over a porous conical surface: A fractional approach", *Results in Engineering*, **26**, p. 104853 (2025). https://doi.org/10.1016/j.rineng.2025.104853
- [35] Zhang, Y., Gao, J., Bai, Y., et al. "Numerical simulation of the fractional Maxwell fluid flow in locally narrow artery", *Computer Methods in Biomechanics and Biomedical Engineering*, **26**(11), pp. 1272–1287 (2023). https://doi.org/10.1080/10255842.2022.2113781
- [36] Huang, J., Chen, L., Li, S., et al. "Numerical study for the performance of viscoelastic fluids on displacing oil based on the fractional-order Maxwell model", *Polymers*, **14**(24), p. 5381 (2022). https://doi.org/10.3390/polym14245381
- [37] Madhura, K.R., Babitha, and Iyengar, S.S., "Impact of heat and mass transfer on mixed convective flow of nanofluid through porous medium", *International Journal of Applied and Computational*

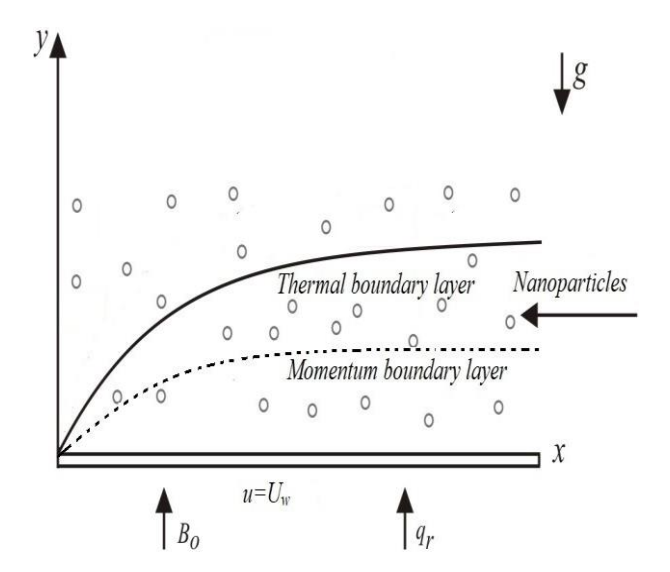


Figure 1: Geometry of the flow.

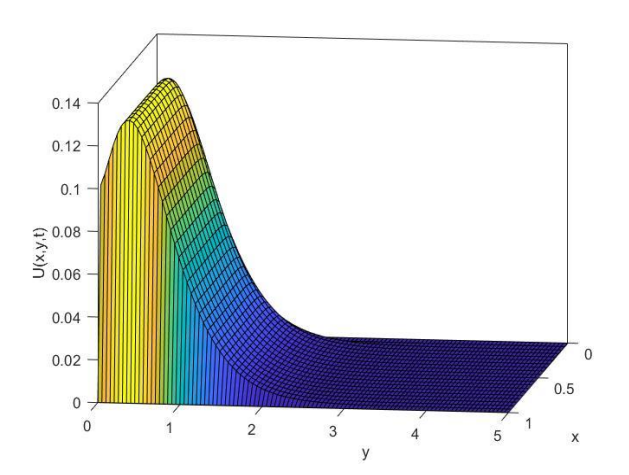


Figure 2: Surface plot of velocity distributions.

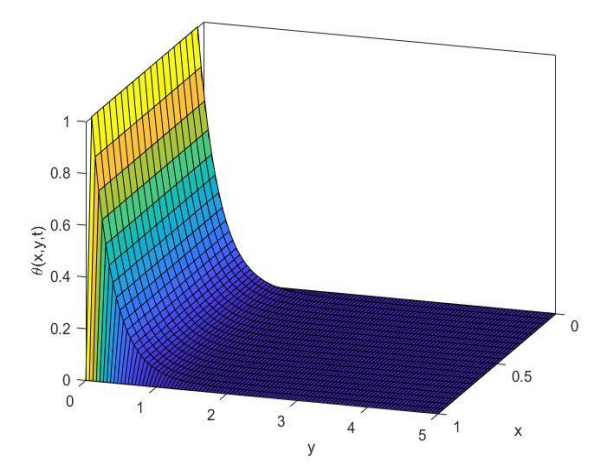


Figure 3: Surface plot of temperature distributions.

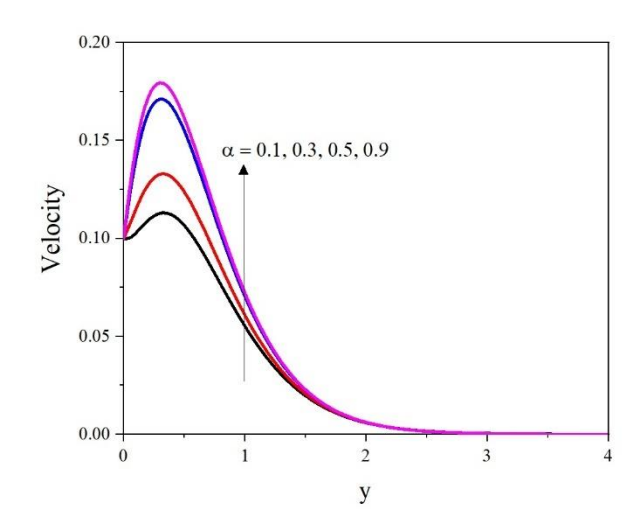


Figure 4: Velocity distributions for various α .

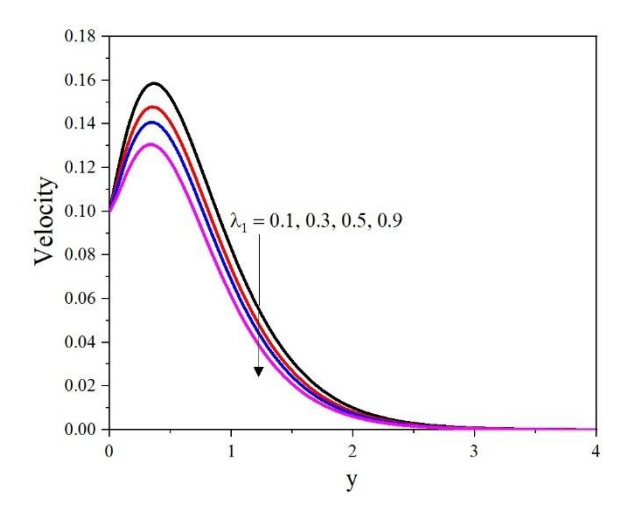


Figure 5: Velocity distributions for various λ_1 .

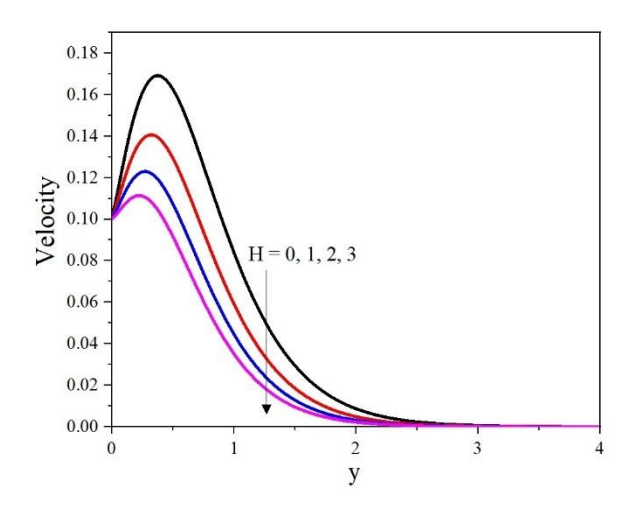


Figure 6: Velocity distributions for various H.

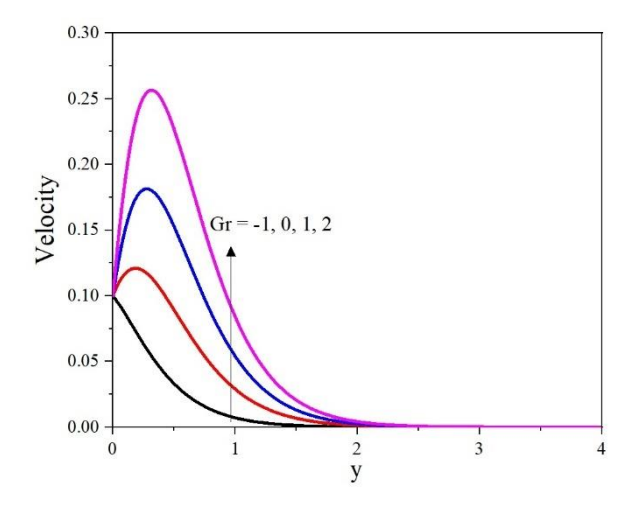


Figure 7: Velocity distributions for various *Gr*.

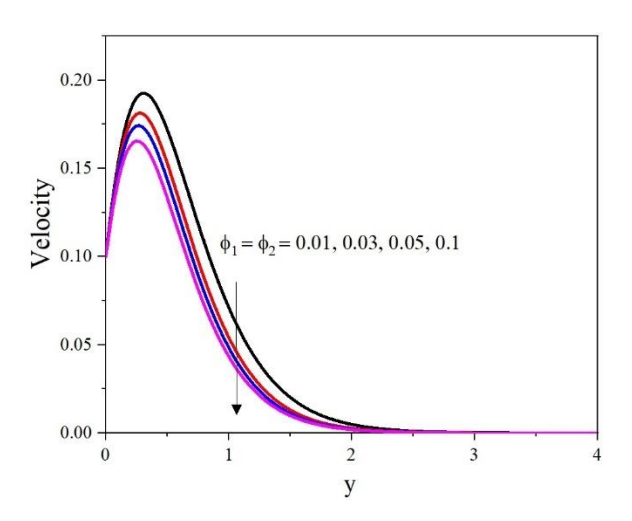


Figure 8: Velocity distributions for various ϕ .

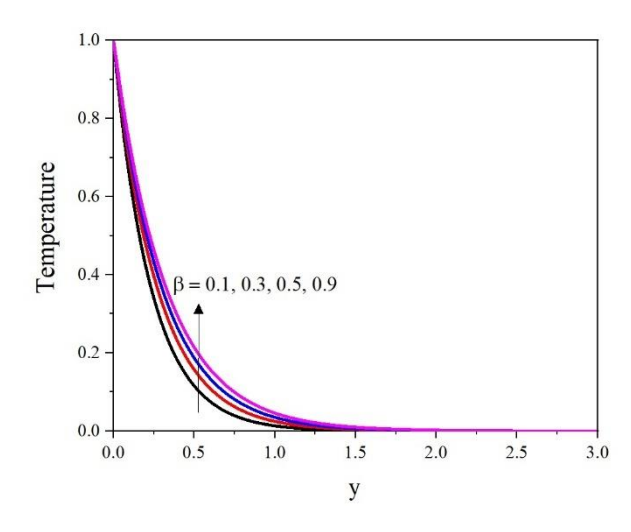


Figure 9: Temperature distributions for various β .

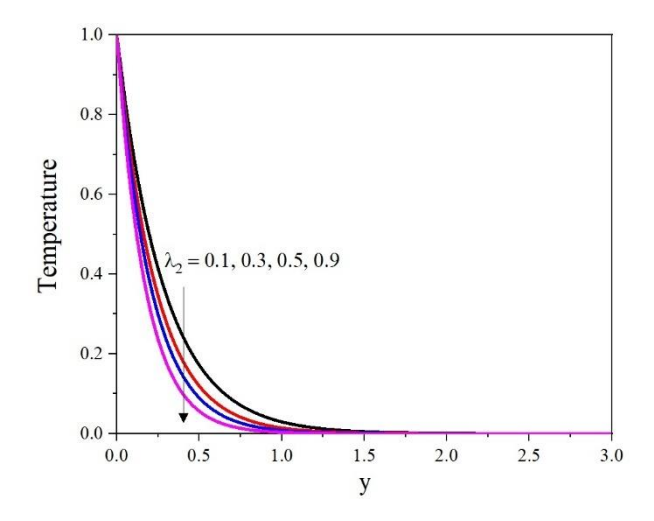


Figure 10: Temperature distributions for various λ_2 .

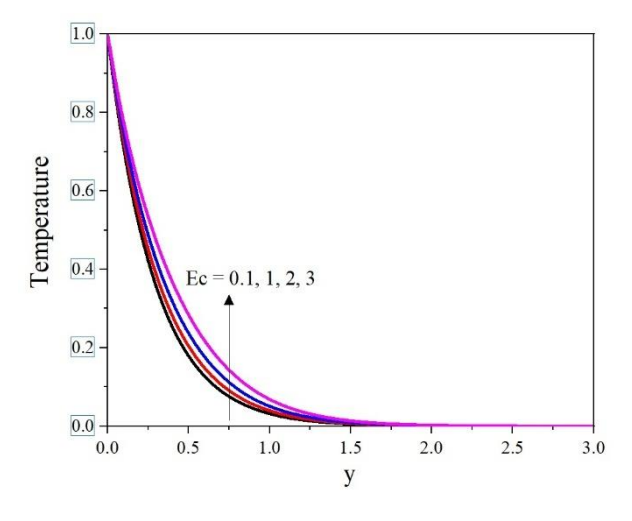


Figure 11: Temperature distributions for various Ec

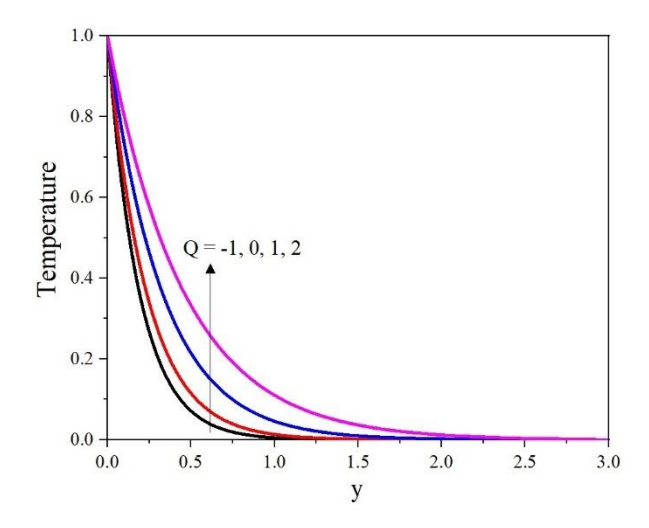


Figure 12: Temperature distributions for various Q

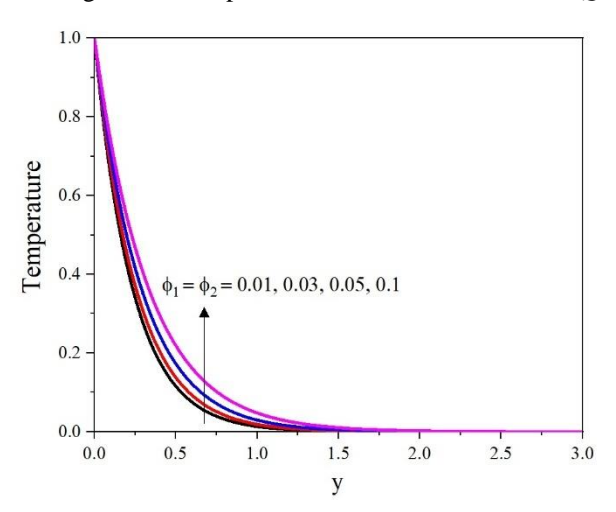


Figure 13: Temperature distributions for various ϕ

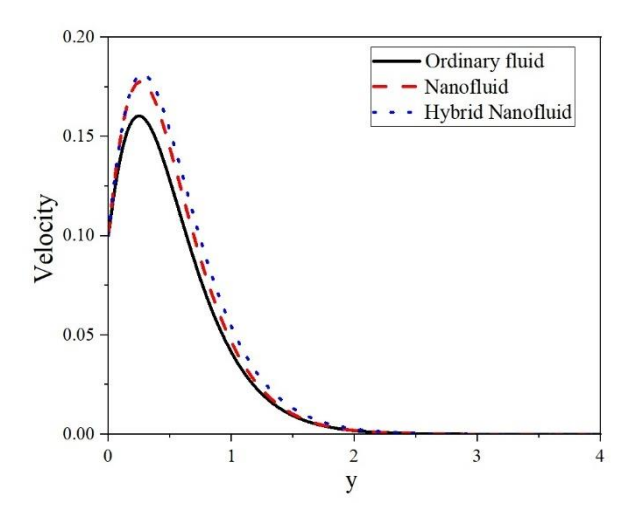


Figure 14: Velocity distributions for various fluids

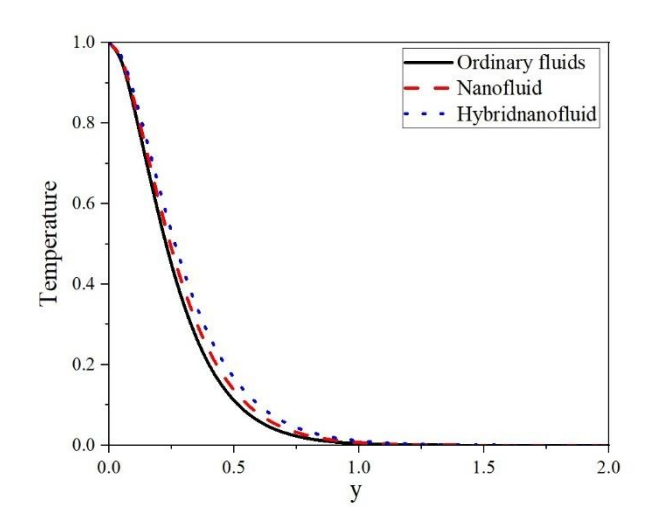


Figure 15: Temperature distributions for various fluids

Table 1: Thermophysical properties of water and different nanoparticles [[6], [2]].

Properties	H_2O	Си	TiO_2
$K(W m^{-1} K^{-1})$	0.613	400	8.9538
$\rho(kg \ m^{-3})$	997.1	8933	4250
$C_p(J \ kg^{-1} \ K^{-1})$	4179	385	686
$B_1 \times 10^{-5} (K^{-1})$	21	1.67	0.9

Table 2: The effective thermophysical properties co-relation of hybrid nanofluid. [24]

Property	Hybrid Nanofluid			
Dynamic Viscosity	$\mu_f = \frac{\mu_f}{(1 - \phi_1 - \phi_2)^{2.5}}$			
Density	$\rho_{hnf} = (1 - \phi_2)[(1 - \phi_1)\rho_f + \phi_1\rho_1] + \phi_2\rho_2$			
Heat Capacity	$(\rho C_p)_{hnf} = \rho_1 \phi_1 C_{p1} + \rho_2 \phi_2 C_{p2} + (1 - \phi_1 - \phi_2) \rho_f C_{pf}$			
Thermal expansion coefficient	$(\boldsymbol{\rho}\boldsymbol{\beta})_{hnf}$ = $(1 - \boldsymbol{\phi}_1 - \boldsymbol{\phi}_2)(\boldsymbol{\rho}\boldsymbol{\beta})_f + \boldsymbol{\rho}_1\boldsymbol{\beta}_1\boldsymbol{\phi}_1 + \boldsymbol{\rho}_2\boldsymbol{\beta}_2\boldsymbol{\phi}_2$			
Thermal Conductivity	$\frac{k_{hnf}}{k_f} = (\phi_1 k_1 + \phi_2 k_2)/\phi + 2(k_f - \phi k_f + \phi_1 k_1 + \phi_2 k_2)$			
	$(\phi_1 k_1 + \phi_2 k_2)/\phi + 2k_f + \phi k_f - (\phi_1 k_1 + \phi_2 k_2)$			

Table 3: Variation of C_f for various parameters

A	λ_1	Н	Gr	$\phi_1 = \phi_2$	C_f
0.1					0.106285
0.5					0.567222
0.9					0.880448
	0.1				0.343763
	0.5				0.567222
	0.9				0.649268
		1			0.567222
		2			0.602321
		3			0.632674
			-1		0.924676
			0		0.805658
			1		0.686543
				0.01	0.536148
				0.05	0.567222
				0.1	0.59205

Table 4: Variation of *Nu* for various parameters

β	λ_2	Ec	Q	$\phi_1 = \phi_2$	Nu
0.1					1.711137
0.5					4.555254
0.9					6.459212
	0.1				0.568497
	0.5				0.711137
	0.9				0.763777
		0.5			0.711137
		1			0.694343
		1.5			0.676919
			-1		2.476369
			0		1.780317
			1		0.711137
				0.01	0.566686
				0.05	0.711137
				0.1	0.8174

Table 5: Comparison of Nusselt number for R=0, $\alpha=\beta=1$, $\lambda_1=\lambda_2=1$, H=0, Q=0, Ec=0, and H=0 for different values of nanoparticle volume fraction.

φ	$Cu - H_2O$ nanofluid		$TiO_2 - H_2O$	nanofluid	
	Ref [30]	Present	Ref [30]	Present	
0	1.40482073	1.404811	1.40482073	1.404811	
0.05	1.50455665	1.504547	1.48088609	1.480876	
0.1	1.60689998	1.606891	1.55782861	1.557819	
0.15	1.71283198	1.712822	1.63613715	1.636127	
0.2	1.82342619	1.823416	1.71632314	1.716313	

Author's Biography:

Dr. Babitha

Dr. Babitha received her Ph.D. in Fluid Mechanics from Visvesvaraya Technological University, Belagavi, Karnataka, India, in 2022. She is currently an Assistant Professor in the Department of Mathematics at CHRIST University, Bengaluru, India. Her research interests include boundary layer flow, heat, and mass transfer analysis of various fluids and heat transfer analysis through fins.

Dr. Madhura K R

Dr. Madhura K. R. is an Associate Professor in the Department of Sciences and Humanities at Swami Vivekananda Yoga Anusandhana Samsthana (S-VYASA), Deemed to be University, Bangalore, Karnataka, India. The author received PhD degree from Kuvempu University, Shankaraghatta, Shimoga, Karnataka, India in the year 2010. Her primary research interests include the study of dusty fluids, nanofluids, and fractional nanofluids, with particular emphasis on heat transfer analysis through extended surfaces such as fins. She has authored 44 research articles in high-impact national and international journals. Dr. Madhura has published 9 patents, written 3 textbooks, and guided more than 30 MSc projects. She completed a major research project funded by the Vision Group on Science and Technology (VGST), Government of Karnataka. Under her supervision, 3 students have completed their PhD degrees, further demonstrating her dedication to academic mentorship and research excellence.